

# Molecular mechanism of atractylon in the invasion and migration of hepatic cancer cells based on high-throughput sequencing

YANG CHENG<sup>1,2</sup>, JIAN PING<sup>1</sup>, JIANJIE CHEN<sup>2</sup>, YIFEI FU<sup>2</sup>, HUI ZHAO<sup>2</sup> and JIAHUA XUE<sup>2</sup>

<sup>1</sup>Institute of Liver Disease, Shuguang Hospital Affiliated to Shanghai University of Traditional Chinese Medicine, Shanghai 201203; <sup>2</sup>Department of Liver Disease, Hospital for Infectious Diseases of Pudong District, Shanghai 201299, P.R. China

Received December 2, 2019; Accepted June 25, 2021

DOI: 10.3892/mmr.2022.12628

**Abstract.** The aim of the present study was to investigate the molecular mechanisms of atractylon in the inhibition of invasion and migration of hepatic cancer cells. High-throughput sequencing was used to compare the expression of long non-coding (lnc)RNAs between hepatic carcinoma and healthy controls. A competing endogenous RNA network was constructed. The top significantly differentially expressed lncRNAs were screened and verified by reverse transcription-quantitative PCR *in vitro* and *in vivo*. Small interfering (si)RNA against thymopoietin-antisense 1 (TMPO-AS1) or coiled-coil domain-containing 183-antisense 1 (CCDC183-AS1) overexpression (oe) vectors were transfected into cells following atractylon treatment. Wound healing and Matrigel assays were used to determine the effects of migration and invasion, respectively. Western blot analysis was used to detect the expression levels of invasion- and migration-related proteins, including N-cadherin, E-cadherin and MMP-2. Flow cytometry analysis was used to detect apoptosis. Based on transcriptome sequencing and analysis, the top seven upregulated [(FAM201A, RP11-640M9.2, AL589743.1, TMEM51-AS1, clathrin heavy chain-like 1 (CLTCL1), TMPO-AS1 and LINC00652] and top six downregulated lncRNAs (RP11-465B22.5, CCDC183-AS1, TCONS\_00072529, RP11-401F2.3, RP11-290F20.1 and TCONS\_00070568) were identified. Only TMPO-AS1 and CCDC183-AS1 were differently regulated by atractylon *in vivo*. The proliferative ability of HepG2 liver cancer cells decreased, whereas the apoptotic rate improved after atractylon treatment. Notably, the invasive and migratory ability of HepG2 cells significantly declined. In addition, siTMPO-AS1

and oeCCDC183-AS1 reduced the effect of atractylon *in vitro*. Atractylon was demonstrated to regulate the expression of TMPO-AS1 and CCDC183-AS1 and inhibited the invasion and migration of liver cancer cells. Thus, TMPO-AS1 and CCDC183-AS1 may be potential targets for diagnosis and treatment of hepatic carcinoma.

## Introduction

Hepatic cancer is a common malignant tumor with the sixth highest incidence rate in the world and third highest rate in China (1). The annual incidence of this disease in China is approximately 20.65 per 100,000, accounting for half of the cases worldwide (2). Hepatic cancer greatly affects the health of the Chinese population; ~300,000 patients succumb to hepatic cancer each year (3). At present, liver transplantation is the main treatment for hepatic cancer, although postoperative recurrence remains an issue (4). The 5-year recurrence rate of hepatic cancer post-surgery is 6% (5). The disease recurs as early as 2 months and most commonly 1-2 years after surgery, thus hindering long-term survival of hepatic cancer patients (6). Therefore, the need to discover new drugs for treating hepatic cancer is particularly urgent.

Atractylon is one of the active constituents in the Traditional Chinese Medicine (TCM) *Atractylodes macrocephala*, belonging to sesquiterpenoids (7). Sesquiterpenoids are widely distributed and are most abundant in the following plants: Magnoliales, rutales, cornales and asterals. In plants, sesquiterpenoids often exist in the volatile oil in the form of alcohols, ketones and lactones, which are also the primary components of the high boiling point of the volatile oil. Previous studies have shown that atractylon exhibits antihypertensive, anti-aging and anti-inflammatory effects (8,9). Hwang *et al* (10) reported that atractylon also serves a role in protection against liver injury. Previous studies have also shown that some TCMs, such as the total extract of *Astragalus* and Baicalin, can exert their unique antitumor effects by inducing apoptosis (11,12). Therefore, the significance of atractylone in cancer treatment requires further investigation.

High-throughput sequencing has been a revolutionary change from traditional approaches, sequencing hundreds of thousands to millions of DNA molecules at a time (13). High-throughput sequencing is widely used to identify

**Correspondence to:** Dr Yang Cheng, Institute of Liver Disease, Shuguang Hospital Affiliated to Shanghai University of Traditional Chinese Medicine, 528 Zhangheng Road, Pudong, Shanghai 201203, P.R. China  
E-mail: drchengyang@163.com

**Key words:** hepatic cancer, atractylon, high-throughput sequencing, invasion, migration, apoptosis

candidate genes for disease and drug therapeutic targets (14). In our previous study, atractylon was reported to induce apoptosis and suppress metastasis *in vivo* and *in vitro* (15). However, the molecular mechanism underlying the inhibitory effect of atractylon on the invasion and migration of hepatic cancer cells required further investigation. Thus, the present study used high-throughput sequencing to explore the mechanisms of action of atractylon in hepatic cancer. By comparing the transcriptome sequencing results of the atractylone treatment and control group, 39 upregulated mRNAs, 39 downregulated mRNAs, 20 upregulated long non-coding (lnc)RNAs and 21 downregulated lncRNAs were identified and screened. In addition, the top 7 differences of lncRNAs (FAM201A, RP11-640M9.2, AL589743.1, TMEM51-antisense (AS)1, clathrin heavy chain-like 1 (CLTCL1), thymopoietin (TMPO)-AS1 and LINC00652] and top six downregulated [RP11-465B22.5, coiled-coil domain-containing 183 (CCDC183)-AS1, TCONS\_00072529, RP11-401F2.3, RP11-290F20.1, TCONS\_00070568) were verified as potential targets of atractylone by *in vivo* and *in vitro* experiments. The results from the present study may provide a theoretical basis for the application of atractylon in the treatment of hepatic carcinoma, and also may provide new potential therapeutic targets for hepatic carcinoma disease.

## Materials and methods

**Cell lines.** HepG2 liver cancer cells were purchased from the American Type Culture Collection (ATCC). By STR identification, cell line was authenticated. The cells were incubated in DMEM (Thermo Fisher Scientific, Inc.) supplemented with 10% fetal bovine serum (FBS; Greiner Bio-One International GmbH) and 1% penicillin/streptomycin in the 5% CO<sub>2</sub> incubator (Thermo Fisher Scientific, Inc.). Cells were passaged three times, then collected by trypsinization and centrifugation at 400 x g and 4°C for 5 min, and separated into three experimental groups (treated with 5  $\mu$ M, 10  $\mu$ M or 20  $\mu$ M atractylon) and a control group. Cells were resuspended in serum-free cell culture medium.

***In vivo* animal tumors.** BALB/c nude mice (n=16; age, 5-6 weeks; weight 18-20 g; male:female n=8/sex) were obtained from Charles River Technology, Inc., maintained under standard laboratory conditions at 25°C with 12-h light/dark cycles, 60% humidity and free access to food and water. The mice are randomly divided into three groups equally, including control group, 5 mg/kg group and 10 mg/kg group. HepG2 cells were subcutaneous injected into the area of the shoulders of the nude mice with cell suspension; a total of 1x10<sup>6</sup> cells in 0.2 ml DMEM medium without FBS was injected. The mice were sacrificed by cervical dislocation after 28 days. The tumor tissues (maximum diameter, 1.71 cm; maximum volume, 956.63 mm<sup>3</sup>) were excised and used to detect the expression of differentially expressed genes. The present study was approved by the Animal Ethics Committee of Shanghai University of Traditional Chinese Medicine (approval no. PZSHUTCM20181001).

**Transcriptome sequencing and analysis.** Transcriptome sequencing and analysis were completed by Shanghai

Majorbio Technology Co., Ltd. (<http://majorbiopharm.bioon.com.cn/>). The HepG2 cells treated with 20  $\mu$ M atractylon (atractylon group; n=3) or without atractylon treatment (control group; n=3) were used for transcriptome sequencing SMART-Seq v4 Ultra Low Input RNA kit (cat. no. 634891; Clontech; Takara Bio USA, Inc.) was used for RNA extraction. An Agilent Bioanalyzer was used to perform capillary electrophoresis; sample quality was evaluated with the RNA Integrity Number (RIN) software algorithm, and the RIN value should be >8. The loading concentration was 100 pmol. Transcriptome sequencing was performed on an Illumina HiSeq sequencing platform. Hiseq2000 with paired-end reads were processed using 150 bp fragments. Image base calling was performed by using the Bcl2fastq v2.17.1.14 (Illumina, Inc.) software on the original image data of the sequencing results. During the sequencing process, the Illumina built-in software determined whether the read should be retained or discarded according to the quality of the first 25 bases of each sequenced fragment. The obtained original sequencing data (Pass Filter Data) results were stored in FASTQ file format, which contained sequence information and corresponding sequencing quality information. Software FastQC (v0.10.1) was used to evaluate the quality of sequencing data. After the test was qualified, the different libraries were mixed according to the requirements of the effective concentration and target off-machine data volume and then perform Illumina HiSeq sequencing. For the original image data of the sequencing results, the base sequence data was obtained by using the Bcl2fastq v2.17.1.14 software (Illumina) for base call recognition and preliminary quality analysis. After quality analysis of sequencing data, Cutadapt v1.9.1 software was used for filtering of sequencing data. Short readings was compared using Hisat2 v2.0.1 software. RNA-seq overall quality assessment were processed, including checking of saturation curve of expression level, examination of RNA-sequencing (RNA-Seq) correlation and detecting of uniform distribution. Then, transcripts were predicted by StringTie v1.0.4 (16) were subjected to variable scission events for classification and expression statistic by ASprofile v1.0.4 software. We used samtools v0.1.18 software for mpileup processing to obtain possible single nucleotide variants results for each sample, and then annotated them with annovar v2013.02.11 software. Based on annovar (v2013.02.11) software (<http://www.openbioinformatics.org/annovar/>), the mutation information was associated with the genetic information to achieve annotation of the mutation site. The transcript sequences of each sample were assembled using StringTie software based on the gene structure annotation file. During the assembly process, the reads of the reference gene segment were preferentially assembled, and a new transcript was constructed for the unread reads. Based on the existing annotation reference files of the human species, the transcript structure information assembled from each sample was combined, deduplicated and optimized using Cuffmerge software to obtain the final reference transcript structure file. At the same time, the gffread software and the genome information of the species were used to extract the sequence information corresponding to these transcripts.

lncRNA identification and prediction involved three steps, including mapped data (StringTie Assembly), transcripts annotations [Filtering known none-long intergenic

non-coding (linc)RNA annotations, filtering transcripts with none-lincRNA characters, filtering transcripts with open reading frames and filtering transcripts with protein-coding potential] and lincRNA annotations. lincRNAs function by binding to DNA, RNA or proteins; some lincRNAs may be precursors to regulatory RNAs, such as microRNA (miRNA) or piwi-interacting RNA. miRanda v3.3a software ([http://cbio.mskcc.org/microrna\\_data/manual.html](http://cbio.mskcc.org/microrna_data/manual.html)) was used to predict miRNA binding sites. The miRanda software uses the following two factors to determine the miRNA binding site, including the degree of sequence complementarity between miRNA and mRNA and the free energy of the formed composite structure. When the miRNA binds to lincRNA or mRNA with a predicted score of score >140 and energy <-20, the combination of the two is more likely. Therefore, searching the database based on miRNA can obtain the relevant binding site. Based on this, the Bedtools intersect method was used for *cis*-mode action target gene prediction, and the Blast v2.3.0<sup>+</sup> software was used to determine the possible *trans*-target genes for lincRNA.

Gene expression levels were positively related with the degree of abundance (the number of copies of the gene in the genome). Both lincRNA and mRNA expression were calculated using Rsem software v1.2.6 (R package), which used the Fragments Per Kilobases per Million Reads (FPKM) method to calculate gene expression levels. Based on the distribution map and box plot of FPKM of all lincRNA genes, the expression levels of lincRNA genes under different experimental conditions were compared. Differential genetic analysis was undertaken using DESeq2 v1.6.3 of the Bioconductor software package. Based on the threshold of absolute  $\log_2FC > 2$  (where FC is fold change) and  $P < 0.05$ , differentially expressed lincRNAs were screened.

Cluster analysis was based on the similarity calculation of data so that genes with the same function or close relationship could be aggregated to identify the function of the unknown gene or the unknown function of the known gene. In the present study, cluster analysis was used to infer whether screened genes were involved in the same metabolic process or cellular pathway. Moreover, cluster analysis was processed for Gene Set Enrichment Analysis (GSEA). Gene Ontology (GO) term enrichment and Kyoto Encyclopedia of Genes and Genomes (KEGG) pathway enrichment were carried out on the differentially expressed lincRNAs and mRNA.  $P < 0.05$  was the threshold to identify significant GO terms/KEGG pathways.

**Reverse transcription-quantitative PCR (RT-qPCR).** RT-qPCR was used to determine the expression levels of the top seven upregulated [FAM201A, RP11-640M9.2, AL589743.1, TMEM51-AS1, CLTCL1, TMPO-AS1 and LINC00652] and top six downregulated [RP11-465B22.5, CCDC183-AS1, TCONS\_00072529, RP11-401F2.3, RP11-290F20.1, TCONS\_00070568] significantly differentially expressed lincRNAs *in vitro* and *in vivo*. For HepG2 cells ( $1 \times 10^4$  cells/cm<sup>2</sup>), the medium in the 6-well plate was aspirated, the cells were washed three times with PBS, 1 ml of TRIzol reagent (Invitrogen; Thermo Fisher Scientific, Inc.) was added to each well, and RNA was extracted according to the instructions. Reverse transcription was carried using the

Table I. List of lincRNA primer sequences used for reverse transcription-quantitative PCR.

lincRNA	Primer sequence (5'→3')
FAM201A	F: GCGTCTCGTGGATATTGCCC R: TGCACGCAATGTGCGAAATCA
RP11-640M9.2	F: GCCGCAAGATGCACTATGTG R: CAAGGTGCTGTGCCAGTCTA
AL589743.1	F: AGCTACAGGCAGGAGGATCA R: AAATCAGGATGGGGTGCAGG
TMEM51-AS1	F: TCCTAATTGCACCCCTGCTG R: GATTCTGGGACCCACCTTGG
CLTCL1	F: GATGGGCATGAATGAGAC R: CGAAGTTGGGAGCAGA
TMPO-AS1	F: AGCATGCTTGTAGGTGACCC R: ATAGCATTGCCAGCCAGTGT
LINC00652	F: GCCCACAAGTGCTATGGACT R: GTTGCTCCACATCCTCACCA
RP11-465B22.5	F: CTCTGCCCTAACCTCCTCCT R: AGGGATGTACCAGGGATGCT
CCDC183-AS1	F: AGTTCTCAGCTCCGTTGCTC R: AAAGGGTGTACTCAGGCTGC
TCONS_00072529	F: GAGACCCTACAGGCCCTACA R: CAAAGTTTTCCAGCCCTGC
RP11-401F2.3	F: CCAAGTATCGAGACTCGCCC R: AGGGCCTGTTCCAGCCTATA
RP11-290F20.1	F: TTCCACGAGTGTTCAGACG R: TCTGGGATTAGGAGGTGGG
TCONS_00070568	F: AGATGGCAAACCCGAGAAGG R: CAAAGCTCCCTCTCCTTGGG
GAPDH	F: ACACCCACTCCTCCACCTTT R: TGACAAAGTGGTCGTTGAGG

AS, antisense; CCDC183, coiled-coil domain-containing 183; CLTCL1, clathrin heavy chain-like 1; F, forward; lincRNA, long non-coding RNA; R, reverse; TMPO, thymopoietin.

PrimeScrip 1st Strand cDNA synthesis Kit (Takara Bio, Inc.) according to the manufacturer's protocol. PCR amplification was performed according to procedure of the Takara amplification kit (Takara Bio, Inc.). The following thermocycling conditions were used for qPCR: Samples were preincubated at 95°C for 20 sec; followed by 40 cycles of 95°C for 10 sec, 60°C for 20 sec and 72°C for 30 sec. Relative expression was quantified using the  $2^{-\Delta\Delta C_q}$  method (16). The primers used for qPCR are provided in Table I. GAPDH was used as an internal reference. The experiments were repeated three times. Total RNA was extracted from 100 mg excised tumor tissues using TRIzol; the subsequent steps were similar to those describe for the cell samples.

**Transfection of small interfering (si)RNA against TMPO-AS1 or CCDC183-AS1 overexpression (oe) vector.** Both siTMPO-AS1 and lentiviral particles of oeCCDC183-AS1 with pLL3.7 plasmid backbone were constructed by Shanghai

Genechem Co. Ltd. Briefly, the pLL3.7 vector was digested with *Xho*I and *Hpa*I, and the linear vector was recovered by electrophoresis, ligated with the siTMPO-AS1 under the action of T4 DNA ligase to construct a recombinant plasmid, transformed into competent *Escherichia coli* DH5 $\alpha$ , and 8 positive clones were screened and identified. The plasmids were extracted, identified by double enzyme digestion, and the positive plasmids were sequenced.

siTMPO-AS1 was transfected into cells by Lipofectamine<sup>®</sup> 2000 (Invitrogen; Thermo Fisher Scientific, Inc.) based on the instruction manual (17). The sequences for si-negative control (NC) and siTMPO-AS1 were as follows: si-TMPO-AS1, sense 5'-GAGCCGAACUACGAACCA ATT-3', and antisense 5'-UUGGUUCGUAGUUCGGCU CTT-3'; si-NC, sense 5'-UUCUCCGAACGUGUCACGUTT-3', and antisense 5'-ACGUGACACGUUCGGAGAATT-3'.

oeCCDC183-AS1 with pLL3.7 plasmid backbone was also constructed by Shanghai Genechem Co. Ltd. For transfection of oeCCDC183-AS1, a single cell suspension was seeded ( $1 \times 10^5$  cells/well) in a 6-well plate and cultured at 37°C for 8 h in a 5% incubator. A total of 20  $\mu$ g oeCCDC183-AS1 recombinant plasmid, 7.5  $\mu$ g pMD2G envelope plasmid, and 10  $\mu$ g pRsv-REV and 15  $\mu$ g pMDLg-pRRE packaging plasmids were dissolved in 100  $\mu$ l sterile ultrapure water and mixed with 180  $\mu$ l Lipofectamine 2000 (Thermo Fisher Scientific, Inc.) to form an transduction complex. Empty plasmid was used as the negative control. All these plasmids were purchased by Shanghai Qifa Experimental Reagent Co., Ltd. The virus supernatant was collected by ultracentrifugation at 4°C for 10 min at 4,000 x g. The virus was diluted and added to HepG2 cells in the culture wells with an MOI of 20. After 12 h of culture, the virus-containing medium was discarded and culture was continued for 96 h, after which overexpression of CCDC183-AS1 was confirmed by RT-qPCR.

**Cell proliferation.** The MTT assay was used to detect the effects of 20  $\mu$ m attractylon treatment and oeCCDC183-AS1 or siTMPO-AS1 transfections on cell proliferation. HepG2 cells at logarithmic phase were seeded on 96-well plates at  $2.5 \times 10^3$  cells/well and incubated at 37°C for 24 h; subsequently, 20  $\mu$ m attractylon, oeCCDC183-AS1 or siTMPO-AS1 were added. The control group was cultured with an equal amount of culture medium; three duplicate wells were set in each group. After incubation at 37°C for 48 h, 29  $\mu$ l MTT (5 mg/ml) was added, and the cells were incubated for an additional 4 h at 37°C. Subsequently, the supernatant was aspirated, 150  $\mu$ l of DMSO was added to each well to dissolve the purple formazan crystals, the plates were shaken with low speed at room temperature for 10 min, and the absorbance at 570 nm was measured using a microplate reader.

**Flow cytometry analysis.** Flow cytometric analysis was used to detect apoptotic rates. Briefly, harvested transfected HepG2 cells were made into single cell suspension ( $1 \times 10^7$  cells/ml), pre-cooled ice-cold 70% ethanol was added and the cells were fixed at -20°C for 24 h. The fixed cells were taken and stained with 5  $\mu$ l Annexin V and 10  $\mu$ l PI (both BioLegend, Inc.) for 15 min at room temperature, and flow cytometry (FACS Calibur; Becton, Dickinson and Company) with the CELLQuest version 6.1.2 software (Becton, Dickinson and

Company) was used to process and analyze the data to calculate the apoptotic rates.

**Wound healing assay.** HepG2 cells at logarithmic phase were digested with 0.25% trypsin to prepare a single cell suspension, and the cell density was adjusted to  $1 \times 10^8$  cells/l. A total of 1 ml cells were seeded into each well of a 6-well plate and cultured in a cell culture incubator at 37°C for 24 h. Once a confluent layer formed, a 100  $\mu$ l pipet tip was used to vertically scrape a wound into the cell monolayer. Cell debris was washed away with PBS, cell culture medium containing 20  $\mu$ l of attractylon and transfection reagent was added. The negative control group was added with an equal volume of cell culture solution. The plate was placed in a 37°C incubator for 24 h; cell migration was observed with an inverted phase contrast microscope, and the width was measured.

**Invasion assay.** After freezing and thawing, the pre-cooled pipette tip was used to mix the matrigel into a homogenate. The culture plate used was placed on ice. After adding Matrigel, the culture plate was placed at 37°C for 30 min. Cell culture medium without FBS and with 5% FBS was in the upper and lower chambers, respectively. Then, the treated cell suspension in each group with  $5 \times 10^4$  cells were added to each well in the upper chamber and cultured for 48 h. The transfected cells were seeded into the upper chamber and incubated in a cell culture incubator for 48 h. The cells on the surface of the filter membrane were carefully scraped off with a cotton swab, and the cells in the 24-well plate were aspirated. Cells on the lower membrane were fixed with 4% formaldehyde and stained with H&E. The cells were observed and photographed using an inverted microscope (Olympus Corporation).

**Western blot assay.** Western blot analysis was used to detect the protein expression levels of invasion- and migration-related proteins, including N-cadherin (N-cad), E-cad and MMP-2. Briefly, cultured cells were washed with PBS pre-cooled to 4°C, then lysed at 4°C in lysis buffer (50 mmol/l Tris-HCl, 1.0 mmol/l EDTA, 150 mmol/l NaCl, 0.1% SDS), incubated for 20 min, centrifuged at 4°C at 12,000 x g for 2 min, and the supernatant was stored at -20°C until used. Protein concentrations were determined by the Bradford method, and the proteins were separated by 10% SDS-PAGE. After electrophoresis, proteins were transferred to a nitrocellulose membrane. The nitrocellulose membrane was blocked in TBST (0.05% Tween-20) (TBST) containing 5% skim milk powder for 90 min at 37°C. Primary antibodies (1:1,000; all from Abcam) against N-cad (cat. no. ab76011), E-cad (cat. no. ab231303) MMP-2 (cat. no. ab51074) and GAPDH (cat. no. ab8245) were added and incubated at 4°C for overnight. After rinsing with TBST, membranes were incubated with HRP-conjugated goat anti-rabbit IgG secondary antibody (cat. no. ab6721, 1:1,000; Abcam) was added at 37°C for 40 min. The membrane was treated with a chemifluorescence reagent (ECL Plus Western Blotting Detection Reagents; Amersham; Cytiva) and detected by the ProXpress 2D Proteomic Imaging System (PerkinElmer, Inc.). The enhanced chemiluminescence system (Pierce; Thermo Fisher Scientific, Inc.) was used for visualization of proteins.



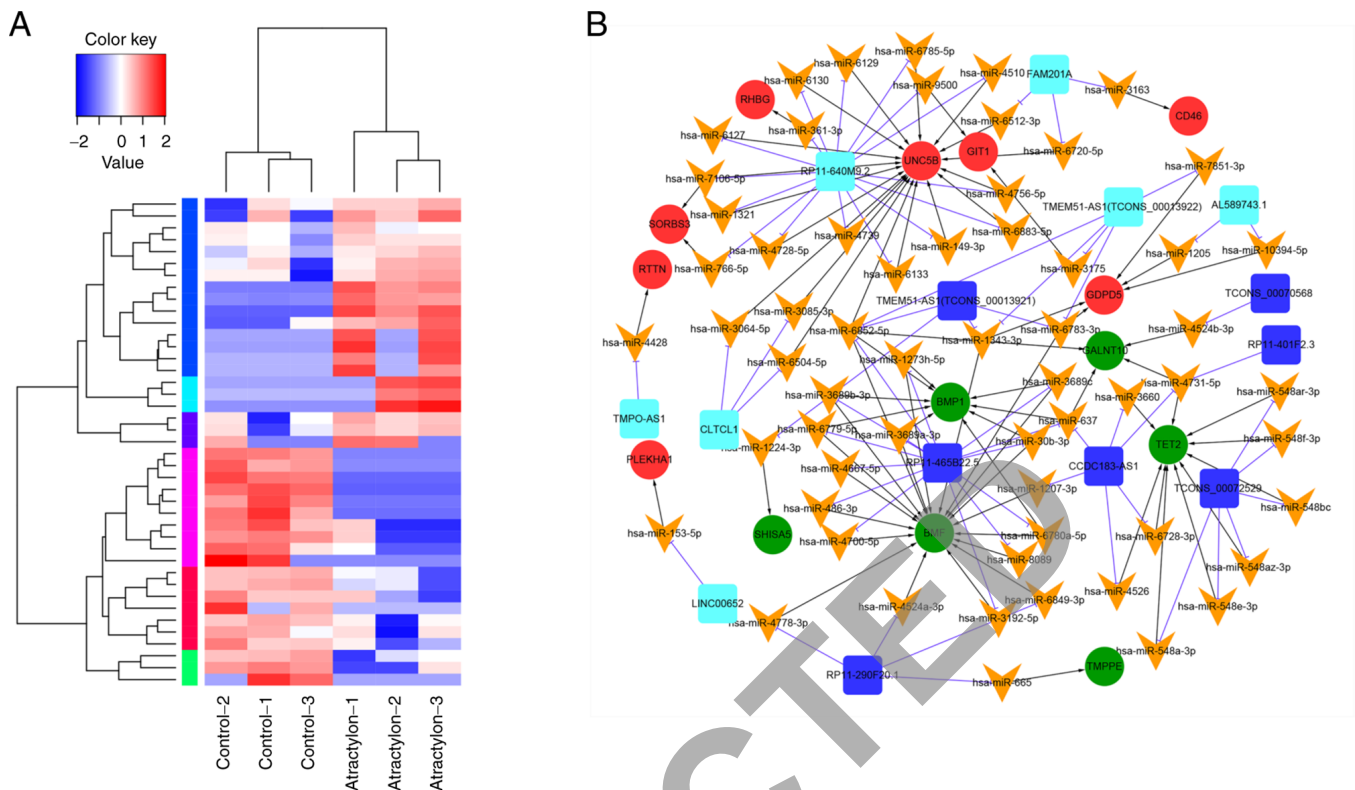


Figure 1. Transcriptome sequencing and analysis. (A) Heatmap of top differentially expressed genes. By comparing the differences between samples by color, the change in the pattern of gene expression between atractylone treatment and control sample groups was assessed. Clustering was performed based on log10 (FPKM+1) values. Red indicates highly expressed genes and blue indicates low expressed genes. (B) Competing endogenous RNA network. A total of 83 lncRNA/miRNA/mRNA relationships were identified, including 61 miRNAs, 13 lncRNAs and 14 mRNAs. The blue square indicates lncRNA, the yellow arrow indicates miRNA, the red circle indicates the upregulated gene and the green circle indicates the downregulated gene. lncRNA, long non-coding RNA; miRNA, microRNA; FPKM, reads per kilobase of exon model per million mapped reads.

**Statistical analysis.** Data are expressed as the mean  $\pm$  standard deviation. Unpaired Student's *t*-test was used to compare the means between the two groups. For multiple groups, one-way ANOVA was performed followed by Tukey's test.  $P < 0.05$  was considered to indicate a statistically significant difference.

## Results

**Differential expression of lncRNAs.** By comparing the transcriptomes of HepG2 cells treated with or without atractylon, a total of 41 differential lncRNA transcript sequences (20 upregulated lncRNAs and 21 downregulated lncRNAs) were screened. The data was uploaded to GEO database with the dataset number GSE165941. Ensembl is a genome browser for vertebrate genomes that supports research in comparative genomics, evolution, sequence variation and transcriptional regulation. A total of 78 differentially expressed mRNA 3' untranslated region (UTR) sequences were downloaded from the Ensembl database (<http://www.ensembl.org>), including 39 upregulated and 39 downregulated mRNAs. miRanda v3.3a software was used to predict miRNA binding sites on the 41 differential lncRNAs and 60 mRNAs. The heatmap in Fig. 1A shows the 219 differentially expressed genes. By comparing the differences between samples by color, the changes in the patterns of gene expression between atractylone treatment and control samples were assessed. A total 219 of lncRNA were screened. Based on the threshold of Score >140

and Energy <-20, a total of 6,262 miRNA-lncRNA pairs were screened, including 41 lncRNAs and 1,769 miRNAs, and total 7,003 miRNA-mRNA pairs were also screened, including 60 mRNAs and 1,981 miRNAs. If there were at least three predicted miRNA binding sites on a lncRNA or 3'UTR sequence of mRNA, the lncRNA or mRNA was regarded as having a targeted regulatory relationship with miRNA. Therefore, 347 miRNA-lncRNA relationship pairs were screened further, including 31 miRNAs and 283 lncRNAs; in addition, 486 miRNA-mRNA relationship pairs were screened, including 31 mRNAs and 392 lncRNAs. To construct a competing endogenous (ce)RNA network, mRNAs and lncRNAs regulated by the same miRNA were screened first. Subsequently, lncRNAs and mRNAs that were simultaneously regulated, were screened out. A total of 83 lncRNA-miRNA-mRNA relationships were identified, including 61 miRNAs, 13 lncRNAs and 14 mRNAs (Fig. 1B). By constructing a ceRNA network, The top 20 upregulated and downregulated lncRNAs are presented in Table II. A total of seven upregulated lncRNAs (FAM201A, RP11-640M9.2, AL589743.1, TMEM51-AS1, CLTCL1, TMPO-AS1, LINC00652) and six downregulated lncRNAs (RP11-465B22.5, CCDC183-AS1, TCONS\_00072529, RP11-401F2.3, RP11-290F20.1, TCONS\_00070568) were identified.

**Gene set enrichment analysis (GSEA).** Cluster analysis was processed for GSEA. Differentially expressed genes were

Table II. Top 20 upregulated and downregulated long non-coding RNAs.

ID	baseMean	log2FoldChange	lfcSE	stat	P-value	padj
TCONS_00070568	9.189601604	-2.658530993	0.617361441	-4.306279625	0.0000166	0.056564093
TCONS_00146228	4.220737895	-2.452311396	0.668385802	-3.669005817	0.000243496	0.414794652
TCONS_00013921	7.78099809	-2.209365086	0.628272498	-3.516571379	0.000437159	0.496467015
TCONS_00162778	104.3997568	0.95057948	0.294023306	3.233007248	0.001224945	0.897074262
TCONS_00247459	3.410420327	-2.135624261	0.669416733	-3.190276186	0.001421369	0.897074262
TCONS_00013922	4.20083662	2.112780528	0.668684551	3.159607208	0.00157982	0.897074262
TCONS_00168315	5.130853259	2.040425289	0.661815739	3.08307157	0.002048759	0.915979734
TCONS_00229320	14.20054823	1.611570425	0.529785881	3.041927848	0.002350682	0.915979734
TCONS_00168994	3.003189856	1.96573041	0.667621772	2.944377329	0.003236052	0.915979734
TCONS_00169826	2.977376421	1.935208347	0.666972896	2.901479744	0.003714048	0.915979734
TCONS_00225882	2.94768661	1.922862646	0.666715391	2.884083181	0.00392555	0.915979734
TCONS_00169170	3.60174634	1.90038175	0.664945797	2.857949864	0.004263878	0.915979734
TCONS_00064235	3.549066177	1.853936582	0.663373502	2.794710035	0.005194628	0.915979734
TCONS_00268181	5.48193499	-1.771181704	0.645927317	-2.74207586	0.006105224	0.915979734
TCONS_00072529	9.052862973	-1.62069798	0.595883352	-2.719824231	0.006531663	0.915979734
TCONS_00259927	3.225820835	1.780974156	0.661410388	2.69269154	0.007087781	0.915979734
TCONS_00211450	3.997141569	-1.735934617	0.667819184	-2.599408133	0.009338467	0.915979734
TCONS_00187111	2.446780778	-1.716612801	0.660586363	-2.598619799	0.009359938	0.915979734
TCONS_00168316	10.58866589	-1.516162448	0.607242559	-2.496798728	0.012532006	0.915979734
TCONS_00218764	2.92919402	-1.577856792	0.667716571	-2.363063703	0.018124554	0.915979734

lfcSE, log fold change standard error; padj, corrected P-value.

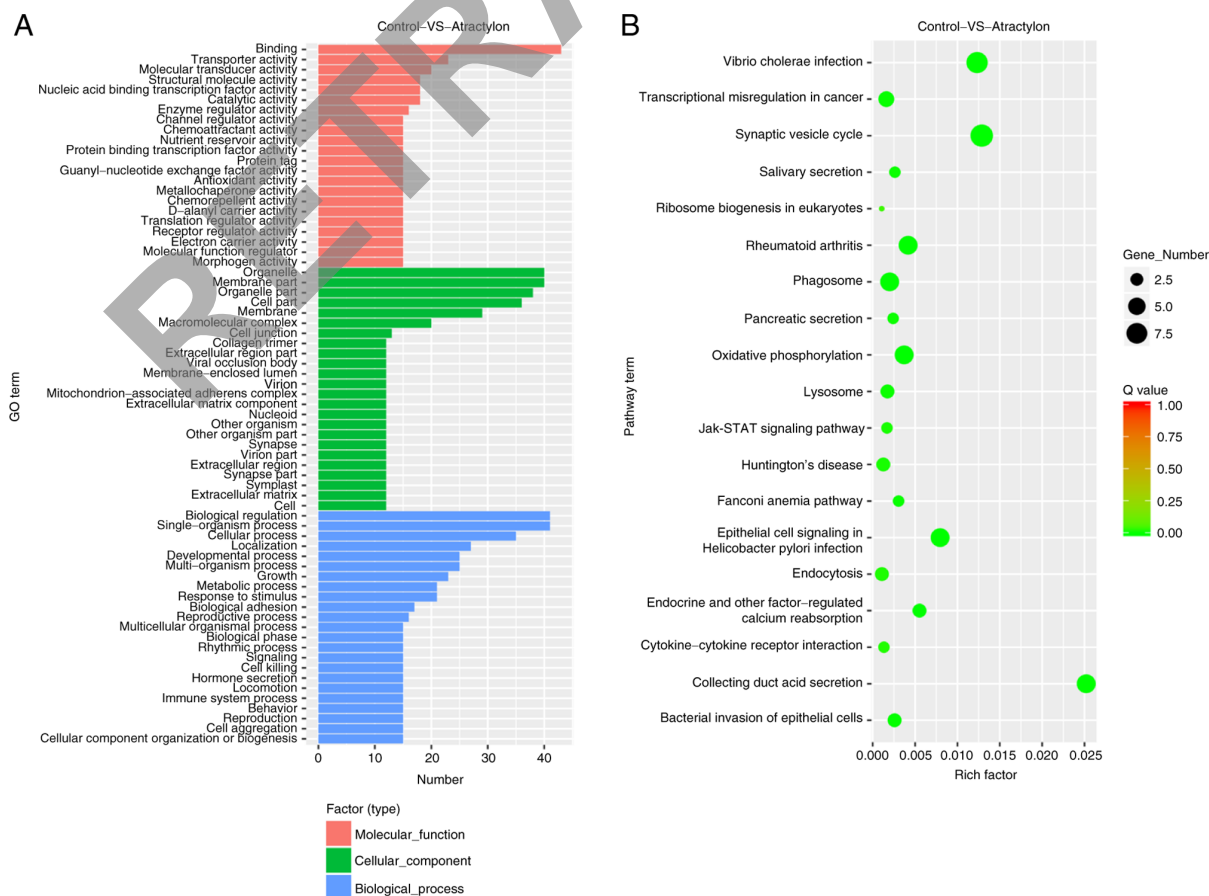


Figure 2. Enrichment of top differentially expressed long non-coding RNAs. (A) Gene Ontology functional term enrichment analysis. (B) Kyoto Encyclopedia of Genes and Genomes pathway enrichment analysis

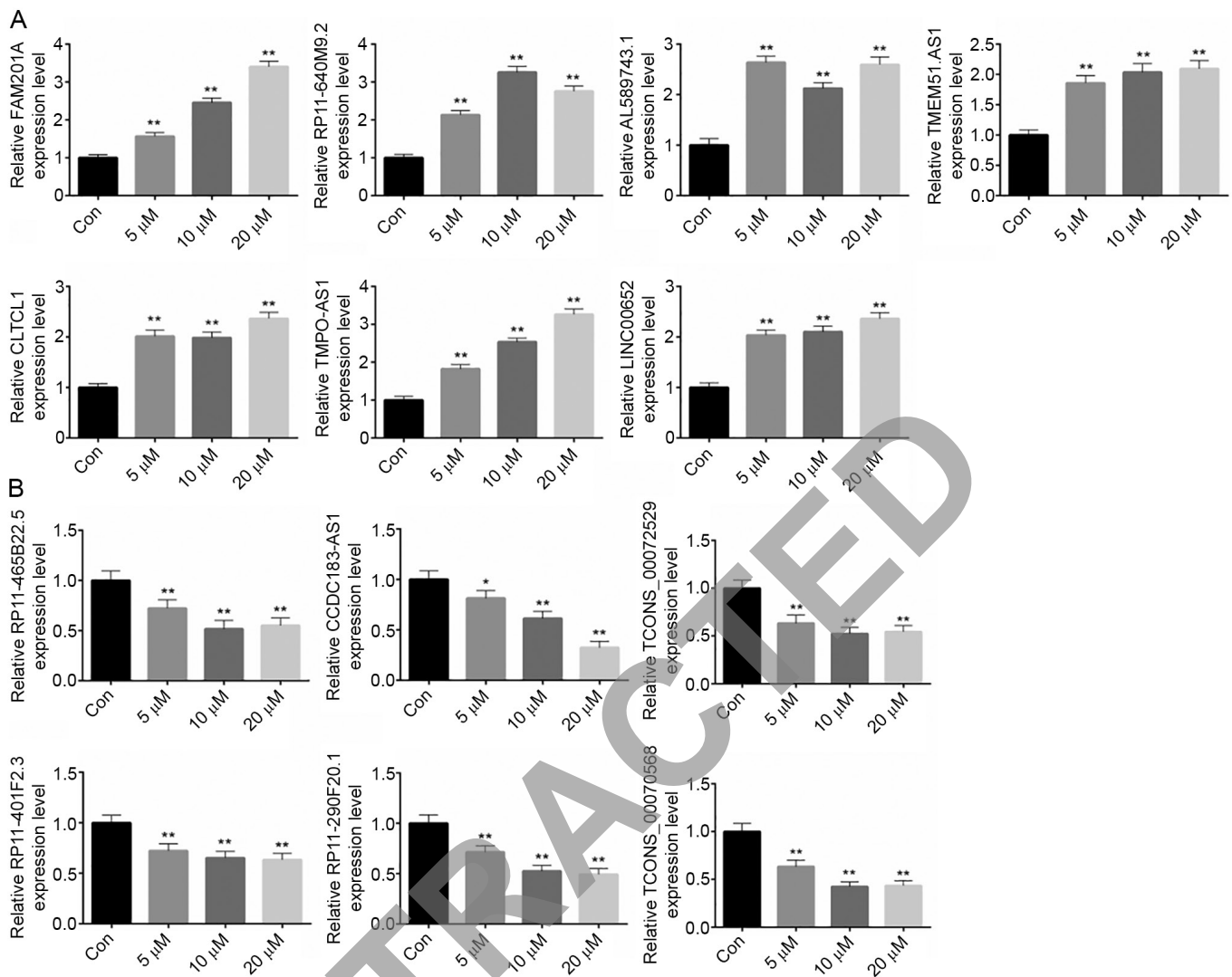


Figure 3. Expression of the top differentially expressed lncRNAs *in vitro*. HepG2 liver cancer cells were treated with 0, 5, 10 or 20  $\mu$ M atractylon. Reverse transcription-quantitative PCR was used to detect the expression levels of the (A) top seven upregulated (FAM201A, RP11-640M9.2, AL589743.1, TMEM51-AS1, CLTCL1, TMPO-AS1, LINC00652) and (B) top six downregulated (RP11-465B22.5, CCDC183-AS1, TCONS\_00072529, RP11-401F2.3, RP11-290F20.1, TCONS\_00070568) lncRNAs *in vitro*. \* $P < 0.05$ ; \*\* $P < 0.01$ . AS, antisense; CCDC183, coiled-coil domain-containing 183; CLTCL1, clathrin heavy chain-like 1; lncRNA, long non-coding RNA; TMPO, thymopoietin.

mainly enriched in the various GO functions, including binding, organelle, membrane, biological regulation and single-organism process (Fig. 2A; Fig. S1). In addition, these genes were also enriched in vibrio cholerae infection, synaptic vesicle cycle, epithelial cell signaling in *Helicobacter pylori* infection, oxidative phosphorylation, jak/STAT signaling pathway and endocrine and other factor-regulated calcium reabsorption (Fig. 2B).

**Expression of the top differentially expressed lncRNAs *in vivo* and *in vitro*.** Cells were divided into four treatment groups, including 0 (control), 5, 10 and 20  $\mu$ M atractylon. Similarly, mice were divided into three treatment groups, including 0 (control), 5 and 10 mg/kg atractylon. RT-qPCR was used to detect the expression of the top seven upregulated (FAM201A, RP11-640M9.2, AL589743.1, TMEM51-AS1, CLTCL1, TMPO-AS1, LINC00652) and top six down-regulated lncRNAs (RP11-465B22.5, CCDC183-AS1, TCONS\_00072529, RP11-401F2.3, RP11-290F20.1,

TCONS\_00070568) *in vitro* and *in vivo*. As shown in Fig. 3A, different doses of atractylon increased the expression of FAM201A, RP11-640M9.2, AL589743.1, TMEM51-AS1, CLTCL1, TMPO-AS1 and LINC00652. Besides, relative RP11-465B22.5, CCDC183-AS1, TCONS\_00072529, RP11-401F2.3, RP11-290F20.1 and TCONS\_00070568 were detected. Moreover, the expression of FAM201A, TMEM51-AS1, TMPO-AS1, LINC00652, CCDC183-AS1, RP11-401F2.3 and TCONS\_00070568 were with dose dependent of atractylon (Fig. 3B). In our previous study, atractylon inhibited hepatic cancer growth *in vivo* (15); however, in the *in vivo* experiments of the present study, only TMPO-AS1 was upregulated (Fig. 4A) and CCDC183-AS1 was downregulated (Fig. 4B) by atractylon. Thereby, the results indicated that atractylon inhibited hepatic cancer growth by regulating TMPO-AS1 and CCDC183-AS1 expression.

*siTMPO-AS1 and oeCCDC183-AS1 reduce the effects of atractylon *in vitro*.* The effects of atractylon on cell

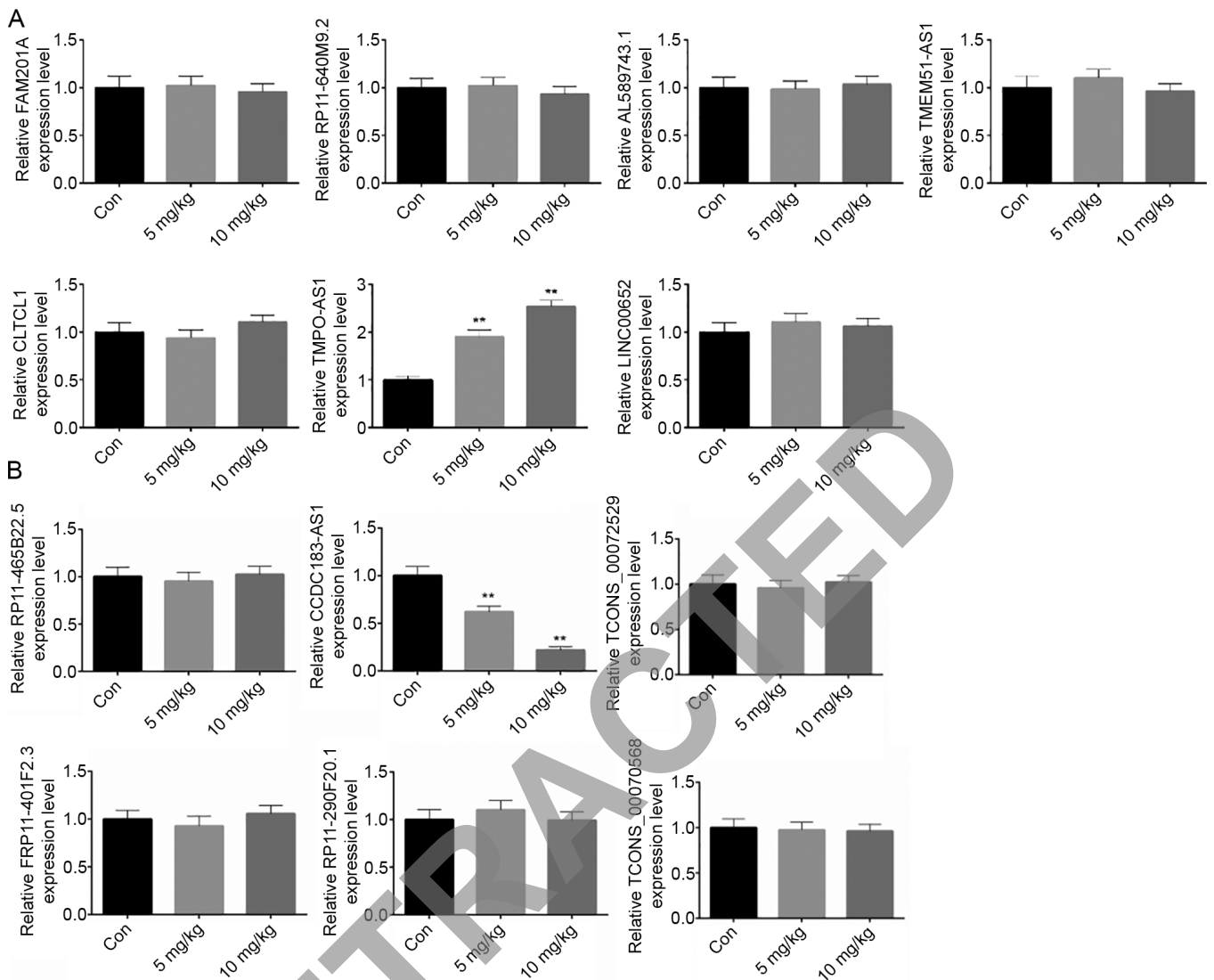


Figure 4. Expression of the top differentially expressed lncRNAs *in vivo*. Expression of the top differentially expressed lncRNAs *in vivo*. Mouse models were divided into three groups, including 0, 5 and 10 mg/kg atractylon treatment groups. Reverse transcription-quantitative PCR was used to detect the expression levels of the (A) top seven upregulated (FAM201A, RP11-640M9.2, AL589743.1, TMEM51-AS1, CLTCL1, TMPO-AS1, LINC00652) and (B) top six downregulated (RP11-465B22.5, CCDC183-AS1, TCONS\_00072529, RP11-401F2.3, RP11-290F20.1, TCONS\_00070568) lncRNAs *in vivo*. \* $P < 0.01$  AS, antisense; CCDC183, coiled-coil domain-containing 183; CLTCL1, clathrin heavy chain-like 1; lncRNA, long non-coding RNA; TMPO, thymopoietin.

proliferation, apoptosis, invasion, and migration were also examined. Based on the aforementioned results, the dose of 20  $\mu$ M atractylon was selected for the following experiments. siTMPO-AS1, oeCCDC183-AS1 and their respective controls were transfected into HepG2 cells and RT-qPCR was used to detect the transfection efficiency; following transfection, TMPO-AS1 was downregulated by siTMPO-AS1, and CCDC183-AS1 was upregulated by oeCCDC183-AS1, indicating successful transfection (Figs. 5A and 6A, respectively). Cells were divided into the following experimental groups: siNC, 20  $\mu$ M + siNC, 20  $\mu$ M + siTMPO-AS1, oeNC, 20  $\mu$ M + oeNC and 20  $\mu$ M + oeCCDC183-AS1 groups. Atractylon treatment significantly decreased the proliferation and increased the apoptotic rate of HepG2 cells compared with the siNC group (Fig. 5B and C, respectively). In addition, the invasive and migratory ability of HepG2 cells significantly decreased following atractylon treatment (Fig. 5D and E, respectively). siTMPO-AS1 transfection was able to reverse the effects of

atractylon *in vitro* (Fig. 5). Based on these data, it was hypothesized that atractylon may inhibit the development of hepatic carcinoma. Similar results were obtained following transfection with oeCCDC183-AS1, including increased proliferation, invasion and migration, and decreased apoptosis of HepG2 cells treated with atractylon (Fig. 6).

**Expression of invasion- and migration-related proteins.** Following treatment with 20  $\mu$ M atractylon with or without siTMPO-AS1 or oeCCDC183-AS1 transfection, the protein expression levels of invasion- and migration-related proteins, N-cad, E-cad and MMP-2, were detected by western blot analysis. As shown in Fig. 7, atractylon treatment significantly reduced the expression levels of N-cad and MMP-2, and increased the expression of E-cad. After siTMPO-AS1 and oeCCDC183-AS1 transfection, the effects of atractylon were reduced compared with the siNC or oeNC group (Fig. 7A and B, respectively).



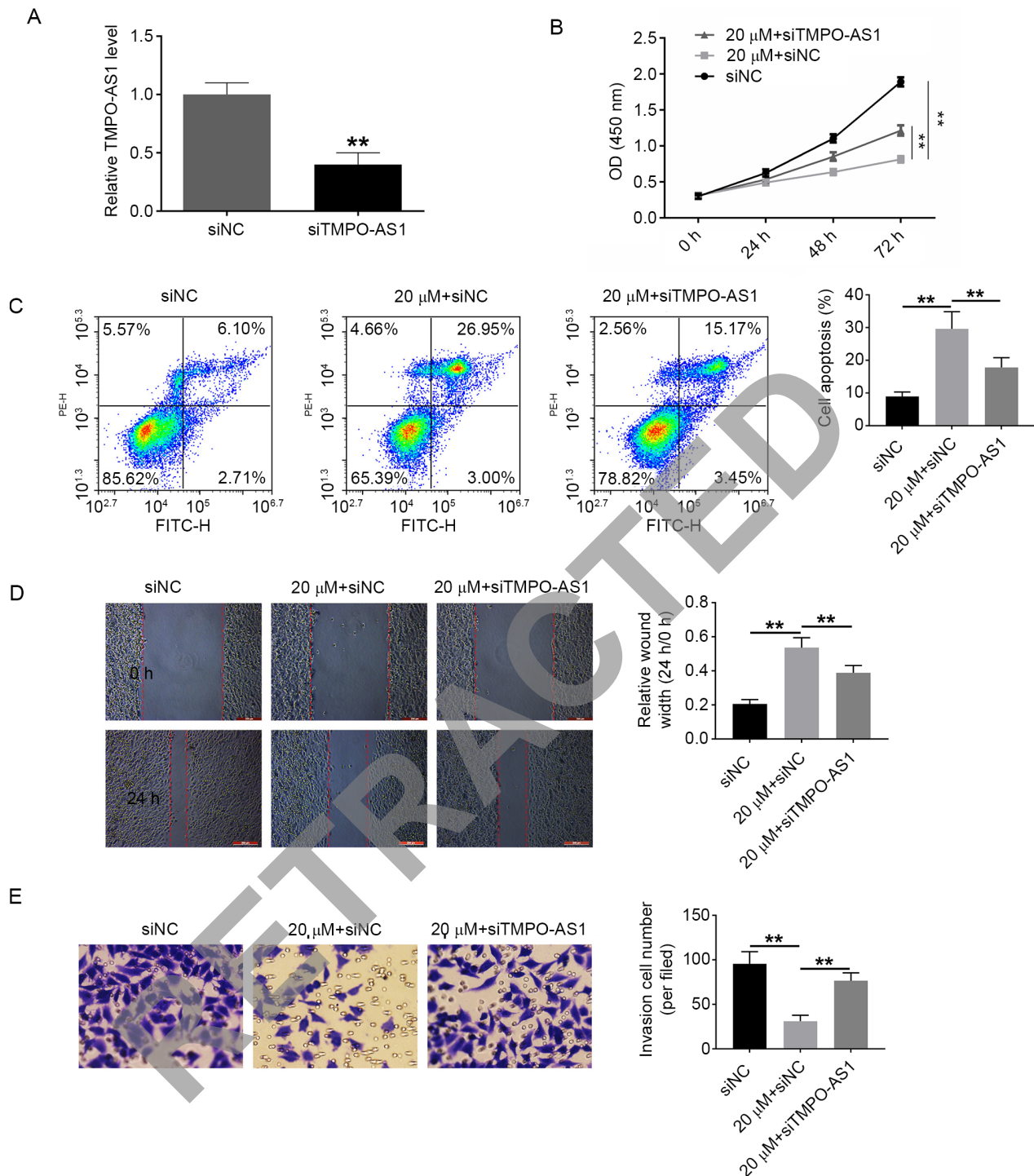


Figure 5. siTMPO-AS1 reduces the effects of atractylon treatment in HepG2 cells. (A) The transfection efficiency of siTMPO-AS1. \*\* $P < 0.01$  vs. siNC. (B) Cell proliferation was detected by MTT assay. (C) Apoptosis was examined by flow cytometry. (D) The migratory ability was determined using a wound healing assay. (E) The invasive ability was detected by Matrigel assay. \*\* $P < 0.01$ . NC, negative control; OD, optical density; si, small interfering RNA; TMPO-AS1, thymopoietin-antisense 1.

## Discussion

Atractylon is a volatile oil extracted from *A. macrocephala* (18). The effects of atractylon on the liver, kidney, spleen and lung have been recorded in the classical pharmacopoeia of China (19,20). Notably, previous studies reported that the drug exhibits anti-oxidation, anti-bacterial, hypoglycemic and antitumor effects (21,22). In the present

study, high-throughput sequencing was used to examine the molecular mechanisms underlying the inhibitory effect of atractylon on the invasion and migration of hepatic carcinoma cells. Based on transcriptome sequencing and analysis, the top seven upregulated (FAM201A, RP11-640M9.2, AL589743.1, TMEM51-AS1, CLTCL1, TMPO-AS1, LINC00652) and top six downregulated (RP11-465B22.5, CCDC183-AS1, TCONS\_00072529, RP11-401F2.3,



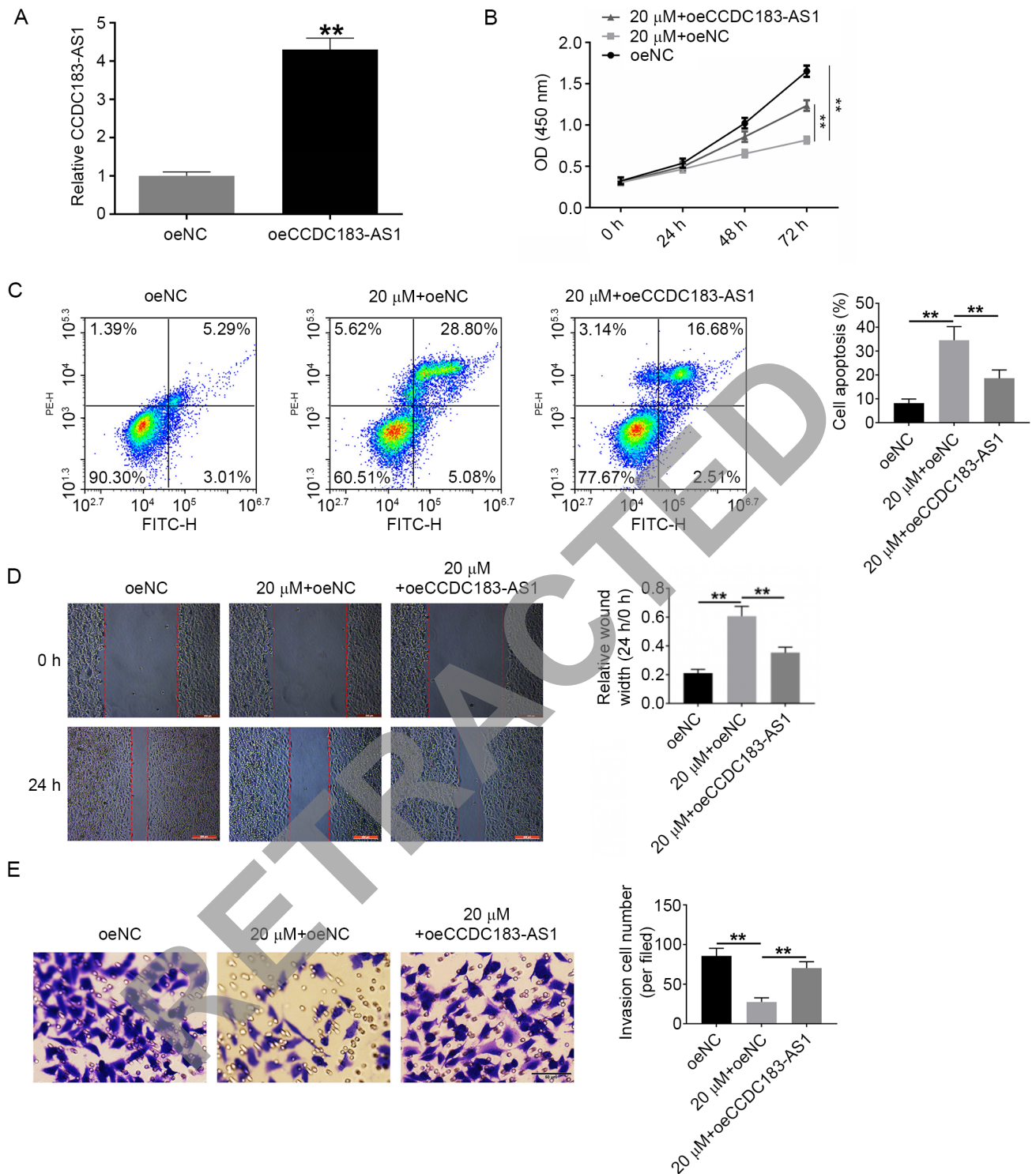


Figure 6. oeCCDC183-AS1 reduces the effect of atractylon treatment in HepG2 cells. (A) The transfection efficiency of oeCCDC183-AS1. \*\* $P < 0.01$  vs. oeNC. (B) Cell proliferation was detected using an MTT assay. (C) Apoptosis was examined by flow cytometry. (D) The migratory ability was determined by wound healing assay. (E) The invasive ability was detected using a Matrigel assay. \*\* $P < 0.01$ . AS, antisense; CCDC183, coiled-coil domain-containing 183; NC, negative control; OD, optical density; oe, overexpression.

RP11-290F20.1, TCONS\_00070568) lncRNAs were identified. The results showed that TMPO-AS1 and CCDC183-AS1 were the only two lncRNAs differently regulated by atractylon *in vivo*, and the molecular mechanism was verified by *in vitro* experiments. Treatment with 20  $\mu$ M atractylon significantly decreased the proliferation of HepG2 cells, the apoptotic rate was increased and the invasive and migratory

abilities were significantly decreased. Transfection with either siTMPO-AS1 and oeCCDC183-AS1 reversed the effects of atractylon *in vitro*.

Atractylon is widely used for cold, arthralgia, edema and phlegm syndrome in Southeast Asian countries (21). Shou *et al* (23) suggested that atractylon could interact with  $E_2$  enzymes and participate the progress of  $E_2$ -P to  $K_E$  reaction.

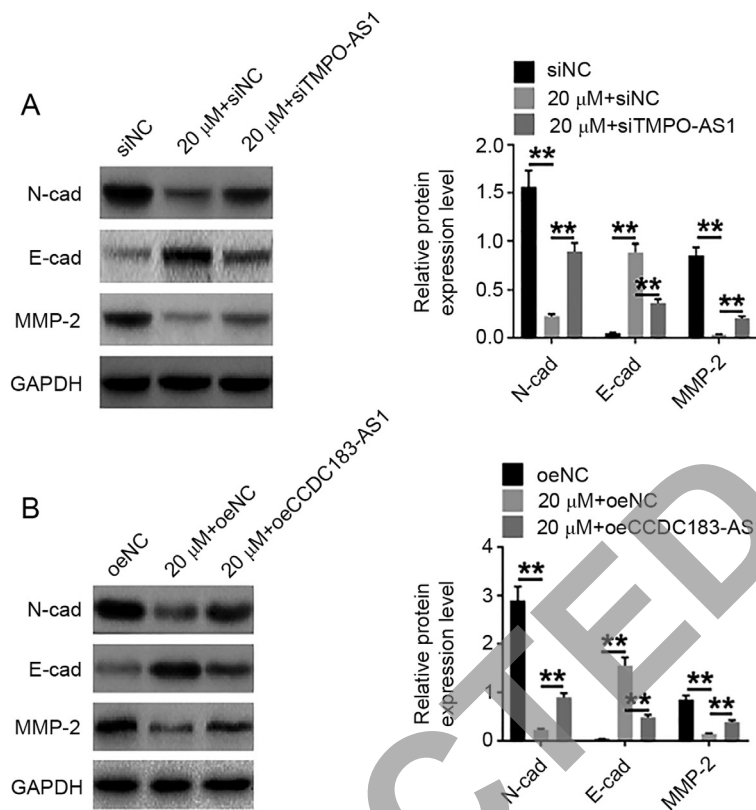


Figure 7. Expression of invasion- and migration-related proteins following atractylon treatment. HepG2 cells were treated with 20  $\mu$ M atractylon with or without (A) siTMPO-AS1 or (B) oeCCDC183-AS1, and the protein expression levels of N-cad, E-cad and MMP-2 were examined by western blotting. \*\* $P < 0.01$ . AS, antisense; cad, cadherin; CCDC183, coiled-coil domain-containing 183; oe, overexpression; si, small interfering RNA; TMPO, thymopoietin.

E2 enzymes participated in synthesis of active ubiquitin, and active ubiquitin was closely related with hepatic cancer and drug sensitivity (24). Atractylon was also reported to have inhibitory effect on tert-butyl hydroperoxide induced DNA damage and hepatic toxicity in rat hepatocytes (10). Therefore, atractylon may be beneficial to the treatment of hepatic disease.

TMPO-AS1 is a 3,254 bp long lncRNA that is expressed in testis [reads per kilobase per million mapped reads (RPKM), 6.1], colon (RPKM, 3.0) and 20 other tissues ([https://db.cngb.org/search/gene/CNGN\\_GENE100128191](https://db.cngb.org/search/gene/CNGN_GENE100128191)). Previous studies have confirmed TMPO-AS1 to be involved in various diseases. For example, Tang *et al* (25) compared lung adenocarcinoma samples and control tissues using bioinformatics, and screened lncRNA TMPO-AS1 as underlying therapeutic target for lung adenocarcinoma treatment. In addition, Li *et al* (26) reported that lncRNA TMPO-AS1 could regulate lung adenocarcinoma cell cycle progression and adhesion, and further influence prognosis of patients with lung adenocarcinoma. lncRNA TMPO-AS1 was confirmed to participate in cell cycle, proliferation, apoptosis and migration, and may represent a prognostic and diagnostic biomarker for prostate cancer (27). TMPO-AS1 also regulates the expression of TMPO and improves the development of non-small cell lung cancer (28). In the present study, TMPO-AS1 was shown to inhibit proliferation, invasion and migration, and improve apoptosis of HepG2 liver cancer cells. In addition, CCDC183-AS1 was identified as a top differently expressed lncRNA; its host gene is 4,922 bp in length and has 5 exons. Results from the present study demonstrated that its

expression was downregulated following atractylon treatment. In addition, CCDC183-AS1 could improve proliferation, invasion and migration, and increase apoptosis of HepG2 cells treated with atractylon. However, the molecular mechanism in has not been investigated to date. Therefore, TMPO-AS1 and CCDC183-AS1 were hypothesized as potential targets of atractylon for hepatic carcinoma treatment.

Moreover, 20  $\mu$ M atractylon treatment was demonstrated to significantly reduce the expression of N-cad and MMP-2 and to increase E-cad expression in the present study. Following siTMPO-AS1 and oeCCDC183-AS1 transfection, the effects of atractylon were reduced. Both E-cad and N-cad are single-chain glycoproteins, which consist of 723-748 amino acids and share 40-60% homology. They are primarily composed of three parts: Extracellular region, transmembrane region and intracellular region. The extracellular region is a signal peptide structure containing calcium ion binding sites, which can specifically bind to calcium ions. The transmembrane zone serves a role in membrane homology, which is the key to establishing and maintaining the polarity of epithelial cells and cell-cell adhesion. Downregulation of E-cad and upregulation of N-cad were observed in a variety of tumors, including melanoma, breast cancer, prostate gland, bladder cancer, colon cancer, and pancreatic cancer (29). A previous study showed that E-cad inhibited cell motility in human epidermoid carcinoma cells by regulating AP-1 family members (30). In addition, methylation or heterozygous deletion of E-cad was closely related to the progression of liver cancer (31). Furthermore,

Lin *et al* (32) confirmed that MMP-2 and its activator membrane type 1-MMP are highly expressed and serve a role in the differentiation of hepatic cancer. Therefore, atractylon may inhibit the invasion and migration of hepatic carcinoma cells.

However, there are some limitations to this study. Firstly, only the top 7 upregulated and 6 downregulated lncRNAs were verified in this study; additional related genes will be investigated in the future. Secondly, expression levels were examined *in vivo*. However, the underlying molecular mechanisms were not explored. Moreover, clinical samples will need to be collected and examined in further studies. Finally, based on the results of the *in vitro* experiment, both 5 and 10  $\mu$ M atractylon were identified as effective doses; however, only three doses were examined. The dose of atractylon *in vivo* will be further researched in the next study.

In conclusion, atractylon was demonstrated to regulate the expression of TMPO-AS1 and CCDC183-AS1, and subsequently inhibited the invasion and migration of hepatic carcinoma cells *in vitro*. Therefore, TMPO-AS1 and CCDC183-AS1 may be potential targets for the diagnosis and the treatment of hepatic carcinoma.

### Acknowledgements

Not applicable.

### Funding

This study was supported by The Key Discipline Construction Projects of Pudong Health Bureau of Shanghai (grant nos. PDZY-2018-0607 and PWZxk2017-30).

### Availability of data and materials

The datasets generated and/or analyzed during the current study are available in the Gene Expression Omnibus repository (GSE165941), <https://www.ncbi.nlm.nih.gov/geo/query/acc.cgi?acc=GSE165941>.

### Authors' contributions

YC conceived and designed the study. JP and JX conducted the experiments. JC analyzed and interpreted the data. YF and HZ performed statistical analysis. YC and JP drafted the manuscript. All authors have confirmed the authenticity of all the raw data, read and approved the final manuscript.

### Ethics approval and consent to participate

The present study was approved by the Animal Ethics Committee of Shanghai University of Traditional Chinese Medicine (PZSHUTCM20181001).

### Patient consent for publication

Not applicable.

### Competing interests

The authors declare that they have no competing interests.

### References

1. An L, Zeng HM, Zheng RS, Zhang SW, Sun KX, Zou XN, Chen R, Wang SM, Gu XY, Wei WW and He J: Liver cancer epidemiology in china, 2015. *Zhonghua Zhong Liu Za Zhi* 41: 721-727, 2019 (In Chinese).
2. Ding C, Fu X, Zhou Y, Liu X, Wu J, Huang C, Deng M, Li Y, Li L and Yang S: Disease burden of liver cancer in China from 1997 to 2016: An observational study based on the global burden of diseases. *BMJ Open* 9: e025613, 2019.
3. Fukui N, Golabi P, Otgonsuren M, de Avila L, Bush H and Younossi ZM: Hospice care in medicare patients with primary liver cancer: The impact on resource utilisation and mortality. *Aliment Pharmacol Ther* 47: 680-688, 2018.
4. Fisher RA, Maluf DG, Wolfe L, Williams B, Cotterell A, Stravitz RT, Heuman D and Posner M: Is hepatic transplantation justified for primary liver cancer? *J Surg Oncol* 95: 674-679, 2007.
5. Pan YX, Chen JC, Fang AP, Wang XH, Chen JB, Wang JC, He W, Fu YZ, Xu L, Chen MS, *et al*: A nomogram predicting the recurrence of hepatocellular carcinoma in patients after laparoscopic hepatectomy. *Cancer Commun (Lond)* 39: 55, 2019.
6. Li J, Wang X, Ma M, *et al*: Liver transplantation for non-hepatocellular carcinoma malignant liver tumors: A single center case study. *Pract J Organ Transplant* 7: 44-47, 2019.
7. Kim HK, Yun YK and Ahn YJ: Toxicity of atractylon and atractylenolide III identified in atractylodes ovata rhizome to dermatophagoides farinae and dermatophagoides pteronyssinus. *J Agric Food Chem* 55: 6027-6031, 2007.
8. Makówka A, Olejniczak-Fortak M and Nowicki M: A comparison of the antihypertensive and anti-inflammatory effects of aliskiren and ramipril add-on therapy in peritoneal dialysis patients-a pilot open label study. *Kidney Blood Press Res* 36: 18-25, 2012.
9. Chen LG, Jan YS, Tsai PW, Norimoto H, Michihara S, Murayama C and Wang CC: Anti-inflammatory and antinociceptive constituents of atractylodes japonica koidzumi. *J Agric Food Chem* 64: 2254-2262, 2016.
10. Hwang JM, Tseng TH, Hsieh YS, Chou FP, Wang CJ and Chu CY: Inhibitory effect of atractylon on tert-butyl hydroperoxide induced DNA damage and hepatic toxicity in rat hepatocytes. *Arch Toxicol* 70: 640-644, 1996.
11. Tin MM, Cho CH, Chan K, James AE and Ko JK: Astragalus saponins induce growth inhibition and apoptosis in human colon cancer cells and tumor xenograft. *Carcinogenesis* 28: 1347-1355, 2007.
12. Tao Y, Zhan S, Wang Y, Zhou G, Liang H, Chen X and Shen H: Baicalin, the major component of traditional Chinese medicine Scutellaria baicalensis induces colon cancer cell apoptosis through inhibition of oncomiRNAs. *Sci Rep* 8: 14477, 2018.
13. Cheng X, Su X, Chen X, Zhao H, Bo C, Xu J, Bai H and Ning K: Biological ingredient analysis of traditional Chinese medicine preparation based on high-throughput sequencing: The story for Liuwei Dihuang Wan. *Sci Rep* 4: 5147, 2014.
14. Nichols AC, Black M, Yoo J, Pinto N, Fernandes A, Haibe-Kains B, Boutros PC and Barrett JW: Exploiting high-throughput cell line drug screening studies to identify candidate therapeutic agents in head and neck cancer. *BMC Pharmacol Toxicol* 15: 66, 2014.
15. Cheng Y, Chen T, Yang X, Xue J and Chen J: Atractylon induces apoptosis and suppresses metastasis in hepatic cancer cells and inhibits growth *in vivo*. *Cancer Manag Res* 11: 5883-5894, 2019.
16. Mane VP, Heuer MA, Hillyer P, Navarro MB and Rabin RL: Systematic method for determining an ideal housekeeping gene for real-time PCR analysis. *J Biomol Tech* 19: 342-347, 2008.
17. Perteau M, Perteau GM, Antonescu CM, Chang TC, Mendell JT and Salzberg SL: StringTie enables improved reconstruction of a transcriptome from RNA-seq reads. *Nat Biotechnol* 33: 290-295, 2015.
18. Cheng Y, Geng L, Wang K, Sun J, Xu W, Gong S and Zhu Y: Long noncoding RNA expression signatures of colon cancer based on the ceRNA network and their prognostic value. *Dis Markers* 2019: 7636757, 2019.
19. Zhao C and He C: Preparative isolation and purification of atractylon and atractylenolide III from the Chinese medicinal plant *Atractylodes macrocephala* by high-speed counter-current chromatography. *J Sep Sci* 29: 1630-1636, 2006.
20. Kiso Y, Tohkin M and Hikino H: Antihepatotoxic principles of atractylodes rhizomes. *J Nat Prod* 46: 651-654, 1983.

21. Cui XB, Shan CX, Wen HM, Wei L and Hao W: UFLC/Q-TOF-MS based analysis on material base of atractylodis macrocephalae rhizoma stir-fried with wheat bran. *Zhongguo Zhong Yao Za Zhi* 38: 1929-1933, 2013 (In Chinese).
22. Cheng Y, Mai JY, Hou TL, Ping J and Chen JJ: Antiviral activities of atractylon from atractylodis rhizoma. *Mol Med Rep* 14: 3704-3710, 2016.
23. Shou D, Dai S, Zhang J, Li H and Yu Z: Simultaneous determination of atractylenolide III, atractylenolide I and atractylon in artactylodis macrocephala using microbore liquid chromatography. *Se Pu* 26: 637-639, 2008 (In Chinese).
24. Satoh K, Nagai F, Ushiyama K and Kano I: Specific inhibition of Na<sup>+</sup>,K<sup>+</sup>-ATPase activity by atractylon, a major component of byaku-jutsu, by interaction with enzyme in the E2 state. *Biochem Pharmacol* 51: 339-343, 1996.
25. Tang DN, Wei JM, Zhu ZM, Wen HX and Guo LY: Experimental study the on relationship between inhibiting the ubiquitin-proteasome pathway and drug sensitivity in human liver carcinoma cell. *Chin J Hepatobiliary Surg* 9: 634-636, 2006 (In Chinese).
26. Li DS, Ainiwaer JL, Sheyhiding I, Zhang Z and Zhang LW: Identification of key long non-coding RNAs as competing endogenous RNAs for miRNA-mRNA in lung adenocarcinoma. *Eur Rev Med Pharmacol Sci* 20: 2285-2295, 2016.
27. Mu X, Wu H, Liu J, Hu X, Wu H, Chen L, Liu W, Luo S and Zhao Y: Long noncoding RNA TMPO-AS1 promotes lung adenocarcinoma progression and is negatively regulated by miR-383-5p. *Biomed Pharmacother* 125: 109989, 2020.
28. Huang W, Su X, Yan W, Kong Z, Wang D, Huang Y, Zhai Q, Zhang X, Wu H, Li Y, *et al*: Overexpression of AR-regulated lncRNA TMPO-AS1 correlates with tumor progression and poor prognosis in prostate cancer. *Prostate* 78: 1248-1261, 2018.
29. Qin Z, Zheng X and Fang Y: Long noncoding RNA TMPO-AS1 promotes progression of non-small cell lung cancer through regulating its natural antisense transcript TMPO. *Biochem Biophys Res Commun* 516: 486-493, 2019.
30. Simsir A, Fetsch P, Mehta D, Zakowski M and Abati A: E-cadherin, N-cadherin, and calretinin in pleural effusions: The good, the bad, the worthless. *Diagn Cytopathol* 20: 125-130, 1999.
31. Andersen H, Mejlvang J, Mahmood S, Gromova I, Gromov P, Lukanidin E, Kriaevska M, Mellon JK and Tulchinsky E: Immediate and delayed effects of E-cadherin inhibition on gene regulation and cell motility in human epidermoid carcinoma cells. *Mol Cell Biol* 25: 9138-9150, 2005.
32. Lin CJ, Lin CY, Wu JC, Huang SH, Wang SM and Chen GH: 357 Macrophage activation promotes invasive properties of hepatocellular carcinoma cells through destabilization of the E-cadherin/B-catenin complex. *J Hepatol* 44 (Suppl 2): S136, 2006.



This work is licensed under a Creative Commons Attribution-NonCommercial-NoDerivatives 4.0 International (CC BY-NC-ND 4.0) License.

RETRACTED